JOURNAL OF THE ROYAL SOCIETY Interface

rsif.royalsocietypublishing.org

Review

Cite this article: Pfeiffer C, Rehbock C, Hühn D, Carrillo-Carrion C, de Aberasturi DJ, Merk V, Barcikowski S, Parak WJ. 2014 Interaction of colloidal nanoparticles with their local environment: the (ionic) nanoenvironment around nanoparticles is different from bulk and determines the physico-chemical properties of the nanoparticles. *J. R. Soc. Interface* **11**: 20130931.
http://dx.doi.org/10.1098/rsif.2013.0931

Received: 11 October 2013
Accepted: 27 November 2013

Subject Areas:
nanotechnology

Keywords:
colloids, screening, ion distribution

Authors for correspondence:
Stephan Barcikowski
e-mail: stephan.barcikowski@uni-due.de
Wolfgang J. Parak
e-mail: wolfgang.parak@physik.uni-marburg.de

†These authors contributed equally to this study.

Royal Society Publishing

Interaction of colloidal nanoparticles with their local environment: the (ionic) nanoenvironment around nanoparticles is different from bulk and determines the physico-chemical properties of the nanoparticles

Christian Pfeiffer[1,†], Christoph Rehbock[2,†], Dominik Hühn[1], Carolina Carrillo-Carrion[1], Dorleta Jimenez de Aberasturi[1], Vivian Merk[2], Stephan Barcikowski[2] and Wolfgang J. Parak[1]

[1]Fachbereich Physik, Philipps Universität Marburg, Marburg, Germany
[2]Center for Nanointegration Duisburg-Essen (CENIDE), University of Duisburg-Essen, Essen, Germany

The physico-chemical properties of colloidal nanoparticles (NPs) are influenced by their local environment, as, in turn, the local environment influences the physico-chemical properties of the NPs. In other words, the local environment around NPs has a profound impact on the NPs, and it is different from bulk due to interaction with the NP surface. So far, this important effect has not been addressed in a comprehensive way in the literature. The vicinity of NPs can be sensitively influenced by local ions and ligands, with effects already occurring at extremely low concentrations. NPs in the Hückel regime are more sensitive to fluctuations in the ionic environment, because of a larger Debye length. The local ion concentration hereby affects the colloidal stability of the NPs, as it is different from bulk owing to Debye Hückel screening caused by the charge of the NPs. This can have subtle effects, now caused by the environment to the performance of the NP, such as for example a buffering effect caused by surface reaction on ultrapure ligand-free nanogold, a size quenching effect in the presence of specific ions and a significant impact on fluorophore-labelled NPs acting as ion sensors. Thus, the aim of this review is to clarify and give an unifying view of the complex interplay between the NP's surface with their nanoenvironment.

1. Introduction

The potential impact of colloidal nanoparticles (NPs) on the environment is a topic of ongoing discussions [1]. The scenario of intended exposure (e.g. fertilizers [2–4], antimicrobial agents [5–7], removal of contaminants [8–10] and clinical use [11–15]), as well as unintended exposure (e.g. contamination [16] and general uptake by all types of organisms [17–20]) has been analysed in a large body of work. These studies clearly point out that in fact NPs have an impact on the environment, whether intended or unintended. However, besides this global impact of NPs on their environment, in a less spectacular way they also influence the physico-chemical properties of their local environment. Likewise, the local environment impacts the physico-chemical properties of the NPs. In this way, there is a subtle interaction between the surface of NPs and their local environment, which affects the physico-chemical properties of both. Important physico-chemical parameters of NP surfaces are for example charge, and hydrophobicity [21]. They are influenced by the local environment (e.g. the surface charge of NPs may depend on the local pH), as the NPs themselves influence the local environment (e.g. accumulations of ions and proteins from bulk

owing to local charge and hydrophobicity patterns). In the following, this will be explained with the example of two major compounds of biological fluids: proteins and salts.

Because many proteins are charged, repulsive interaction between proteins and NPs (for like-charged NPs and proteins) or electrostatic attraction (for oppositely charged NPs and proteins) can occur [22,23]. NP surfaces may also contain local hydrophilic/hydrophobic patterns that cause protein adsorption [24,25]. This layer of adsorbed proteins to the surface of NPs has been termed protein corona [26,27]. Continuing our aforementioned argument, the formation of the protein corona (i.e. interaction between NPs and proteins [28]) affects both, the NPs, as well as their local environment. Adsorbed proteins clearly change two key parameters of NPs: their hydrodynamic diameter [29,30] and in many cases also their colloidal stability [31–33]. On the other hand, the NPs may also affect (some types of) adsorbed proteins, in particular via structural changes, which may lead to dysfunction of the proteins [34–36]. In addition, owing to local charge and hydrophobicity [37] effects associated with the NP surface, there is a higher local protein concentration present on the NP surface (the corona) than in bulk, and thus high NP concentrations can deplete bulk solutions from proteins. Adsorption of proteins to NPs can be experimentally assessed with a variety of different methods, some of which are specific to the NP nature. One example is size measurements of the NPs [38–40]. The more protein molecules are adsorbed on the NP surface, the bigger the size of each NP becomes [29,41,42]. In the case of highly colloidal stable NPs with narrow size distribution, it was shown that in solutions with only one type of protein (such as for example human bovine serum [29,43] or transferrin [30,44]) adsorbed proteins under saturation conditions form a monolayer on top of the NP surface. Often, interaction of proteins with NPs is unwanted and thus needs to be circumvented. Protein adsorption to surfaces is for example reduced by controlled pre-saturation of the surface with serum albumin, which blocks adsorption spots and thus reduces adsorption of other proteins. The PEGylation (poly(ethylene glycol), PEG) of NPs is also used as a general and effective approach to reduce non-specific binding of proteins to NPs [45].

Also interaction of salt and NPs has an effect on the NPs, as well as on the local concentration of the ions (from the dissociated salt). The surface charge of NPs plays also an important role on the stabilization of NPs. In order to prevent agglomeration by van der Waal's attraction, NPs need to be stabilized either by electrostatic or by steric repulsion [46–48]. In the case of electrostatically stabilized NPs, the NPs with likewise charged surfaces repel each other and thus are dispersed. Salt in solution screens the charge on the NP surface (basically in first order by the Debye–Hückel effect [49]), and thus typically leads to colloidal instability at high concentrations, followed by agglomeration [50–54]. While this screening effect (e.g. the effect of the local ion concentration on the colloidal stability of NPs) is reported plentifully in the literature, another consequence of the same effect is less widely reported, but not less relevant. In case, the charge on the surface of the NPs is screened by counter ions, there is a higher and lower concentration of ions with the opposite and the same sign of charge around the NPs compared with bulk, respectively. Thus, the NPs change their local environment, and ion concentrations at the NP surface are different from bulk [55–57]. Local ion concentrations around NP surfaces can be measured using for instance ion-sensitive fluorophores [55–57]. The theoretical analysis however is not as straightforward. When interactions of ions with the curved nanoenvironment of NPs are generally discussed, most applied models, e.g. the Derjaguin–Landau–Verwey–Overbeek (DLVO) theory [58,59] are based on continuum effects considering ions as point charges [60]. However, effects considering the nature of the used ions, namely *specific* ion effects, are often disregarded, though they may be of high importance for example for the colloidal stability of the NPs. These effects have long been known for example in biological systems, in which they are responsible for the well-known Hofmeister effect [61–64], describing stabilization and precipitation tendencies in proteins. Another example is the well-known fact that specific adsorption and monolayer formation of anions occurs in flat charged gold surfaces dipped in electrolytes [65–69]. Hence, ion-specific effects must not be ignored when the nanoenvironment of NPs is studied, particularly at low salinities in case the previously discussed screening of charges described by continuum models is not dominant. Changes in the ion concentration around the surface of NPs have a profound effect on ion-sensitive NPs, as instead of the bulk ion concentration the local ion concentration is determined [55–57].

Thus, interaction of ions and proteins with NPs affects both the ions and proteins as well as the NPs. In the following, we will focus on the case of ions.

2. Non-specific effects of ion-induced nanoenvironments on the synthesis and stability of ligand-free metal nanoparticles

The nanoenvironment of charged NPs has been extensively studied for a long time. Generally, the model of the electrochemical 'double layer' by Stern [70,71] which describes a fixed layer of surface charges (the Helmholtz model [72]), and a continuous diffuse layer of counter-ions (the Gouy–Chapman model [73–75]) is used in this context. The thickness of this diffuse layer, and hence the nanoscopic vicinity of the NPs, is highly dependent on the solution's ionic strength and may be characterized by the Debye parameter (κ) or its reciprocal value, the Debye screening length (κ^{-1}). In a classical DLVO model [58,59], which considers dissolved ions as point charges, κ^{-1} decreases with increasing ionic strength (I[M], which is a function of the concentration of all ions: $I = 1/2 \sum_i z_i^2 c_i$, where z_i is the valence of ions of species i, and c_i [M] the respective concentration of these ions). This leads to a screening of surface charges accompanied by a reduction of the electrostatic stability and induces NP agglomeration owing to dominant van der Waal's attraction. Next to these frequently described effects, the nanoenvironment also affects the electrophoretic mobility (μ [$m^2V^{-1}s^{-1}$]) of NPs and hence related values, such as the zeta-potential (ζ [V]), a parameter of utmost importance when judging NP stabilities in colloidal science [76]. The main parameters in this context are the ionic strength, influencing the Debye parameter (κ [m^{-1}]), and the NP radius (r_c [m]). Based on these values, the best representation of the correlation between μ and ζ may be given by the Smoluchowski formula [77] for the nanoenvironment of larger NPs at high ionic strengths ($\kappa \times r_c \gg 1$) and by the Hückel equation [78] for low ionic strengths and small NPs ($\kappa \times r_c \ll 1$). In the intermediate regime, the Henry function $f_H(\kappa \times r_c)$ may be used [79]. Please note that we are referring

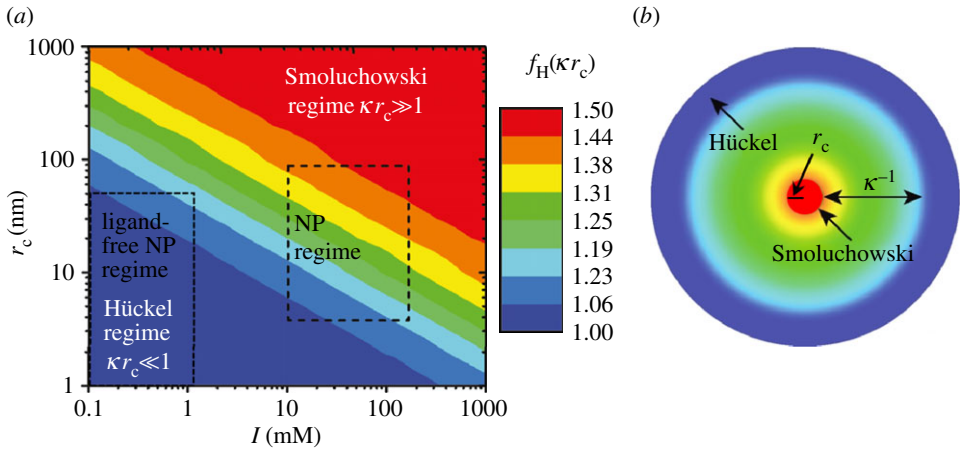

Figure 1. (*a*) Scheme showing different models for the determination of the electrophoretic mobility of bare NPs for different ionic strengths *I* and NP radii r_c (referring to the geometrical radii of the inorganic NP materials). The colour indicates the Henry factor f_H, which defines the relationship between the bare mobility μ and resulting zeta-potential ζ, with higher zeta-potentials at given mobility in the Hückel regime. Note that f_H changes with the distance from the NP surface. (*b*) Shows the two-dimensional distribution of the Debye layer thickness κ^{-1} (adapted from Doane *et al.* [76]).

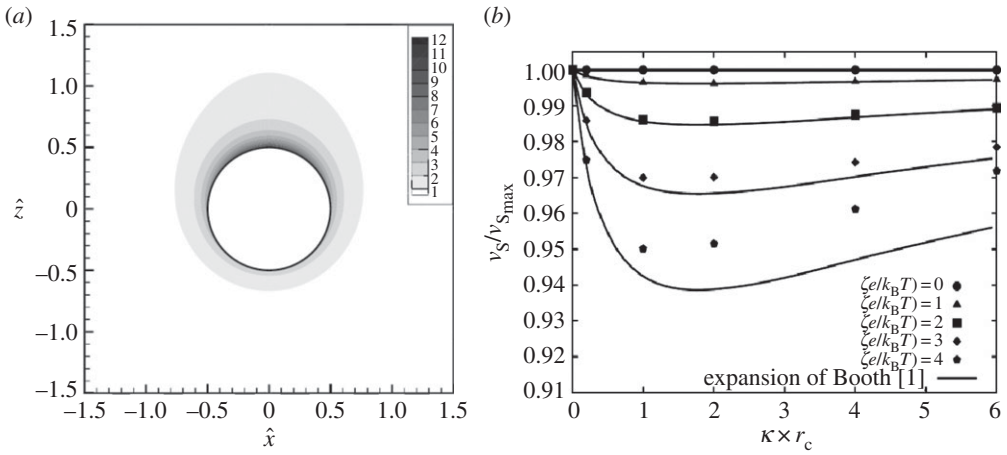

Figure 2. Distortion of the ionic nanoenvironment during centrifugation and effect on the sedimentation velocity v_S at different zeta-potentials ζ. (*a*) Distribution of counter-ions around an NP in the *x*–*z* plane at $\kappa \times r_c = 2$, $\zeta e/k_BT = 3$, and a fluidic Reynolds number of $Re_f = 4.45 \times 10^{-2}$ (100 000 g). (*b*) Normalized sedimentation velocity $v_S/v_{S_{max}}$ at different $\kappa \times r_c$ and $(\zeta e/k_BT)$ values (adapted from Keller *et al.* [85]).

to (geometrical) particle radii r_c, not to hydrodynamic radii r_h [21]. A more detailed discussion of the different models can be found in a review article recently published by Doane *et al.* [80]. Figure 1 shows the different regimes dependent on NP radius r_c and ionic strength *I*. With the zeta-potential ζ being inversely proportional to the Henry factor, zeta-potentials of an NP at a given mobility μ are up to 50% higher ($f_H = 1.5$) in the Hückel regime. NPs synthesized by wet chemistry methods typically bear charge and mobility properties in the intermediate regime (marked in figure 1) between Smoluchowski and Hückel [76], whereas colloids with low ionic strength, e.g. physically prepared colloidal NPs [81–84], are often located in the Hückel regime, being more sensitive for local changes or fluctuations in the ionic environment as a result of the larger Debye length κ^{-1}. Note that ion adsorption to the surface of NPs results in a non-continuum ionic strength regime around the NPs, causing a gradient in the Henry factor. In ideal conditions (no drag force, very low or very high fluid Reynolds numbers), the two-dimensional distribution of the Henry factor around the NP is symmetric.

Next to external electrical fields, the symmetric vicinity of an NP may also be altered by gravitational forces as they are found during centrifugation. A detailed understanding of this process and its correlation with ionic strength, *g*-force and zeta-potential may help to elucidate the sedimentation process and might contribute to controlling agglomeration processes occurring during centrifugation. Recent simulation experiments conducted by Keller *et al.* [85] revealed that the counter-ion cloud found in the vicinity of the NPs is deformed at high *g*-forces (figure 2*a*). This leads to a local electric field which causes a reduction in the sedimentation velocity v_S [m s^{-1}]. This process is highly dependent on the present zeta-potential ζ and the ionic strength *I*. This correlation is depicted in figure 2*b*, where ζ is shown as the dimensionless factor $\zeta e/k_BT$, where *e* is the elemental charge ($e = 1.602 \times 10^{-19}$C), k_B is the Boltzmann factor ($k_B = 1.380 \times 10^{-23}$ J K^{-1}), and *T* [K] is the temperature of the solution. In that context, a factor of 1 at room temperature ($T = 298$ K) is equivalent to a zeta-potential of 26 mV. The ionic strength is plotted as the factor $\kappa \times r_c$, where a value of 2 is equivalent to an ionic strength of 1.04×10^{-6} M at a particle radius of $r_c = 3 \times 10^{-7}$ m.

The preceding examples clearly demonstrate that the continuous, ion-induced nanoenvironment can remarkably alter the physical properties of NPs and may have a severe influence on colloidal chemistry. These effects are meant to be particularly pronounced at ligand-free particles, which hence could

provide a sufficiently sensitive system to study such effects. However, in the above described examples, the ions were only considered as point charges and ion-specific effects were not yet considered [60]. The point of ion specificity is further addressed in the following paragraph.

3. Specific effects of ion-induced nanoenvironments on the synthesis and stability of ligand-free metal nanoparticles

The specific impact of ions on bare noble metal surfaces has been widely studied for decades, e.g. for gold electrodes in the presence of different electrolytes. A significant accumulation and adsorption of the halogens Cl^-, Br^- and I^-, and hence changes of the nanoenvironment have been reported and verified by several methods, including atomic force microscopy [68], X-ray diffraction analysis [67], scanning tunnelling microscopy [66] and surface enhanced Raman scattering [65]. Additionally, it has been known for a very long time that bare gold surfaces dipped in pure water suppositionally collect a negative surface charge owing to accumulation of OH^- [69]. Another example of specific ion interactions is the Hofmeister effect, which has been known since the nineteenth century [62]. It was first discovered in the field of protein precipitation [61,63,64], but was successfully applied to other fields, ranging from simple physical effects on electrolytes to colloidal dispersions and macromolecules [86]. This effect is based on the fact that ions may be classified into chaotropic (soft) and kosmotropic (hard) based on their stabilization of biomolecules and their interactions with surfaces. The nature of these effects is not yet fully understood but it is believed that it may be related to the polarizability of the ions [87,88]. While chaotropic ions have a diffuse charge distribution, they may interact with hydrophobic surfaces, whereas kosmotropic ions with a high surface charge density are repelled. Other findings seem to indicate that the structure of the water molecules found on their surface may be of paramount importance. While water molecules close to kosmotropic ions are highly ordered, chaotropic ions are known to alter their surrounding water shell [89–91]. Hence, ions may lose their hydrate shell and become chemisorbed on hydrophobic surfaces, which is not possible for densely hydrated kosmotropic anions [92]. Even though ion-specific effects have been discussed for a very long time, a detailed examination and transfer of these effects to the nanoenvironment of NPs has long been neglected owing to the unavailability of appropriate test systems. NPs obtained from gas-phase synthesis are barely available in colloidal state owing to their strong agglomeration tendencies and hence undefined surface areas [93,94]. On the other hand, ion-induced interactions with metal surfaces are screened in the presence of surface ligands such as citrate [95] negating a study of these effects with chemically synthesized NPs. In this case, ion–NP interactions in the nanoenvironment are dominated by the nature of the organic ligands, which is thoroughly discussed in the next paragraph. Most recently, the availability of ligand-free colloidal NPs synthesized by the quickly emerging field [82,96] of pulsed laser ablation in liquid [83,84,97,98] has significantly stimulated this research, whereas particularly gold colloids were extensively studied [96,99,100]. Owing to this emerging synthesis route, ultrapure curved NP surfaces are nowadays available which enable studies of NP–ion interactions in the Hückel regime at extremely low ionic strengths [31,101]. These effects will be thoroughly reviewed in the following and complemented by some recent findings. Basically, these effects can be subdivided into (i) ion effects, and (ii) pH effects though in many experiments this influence cannot be clearly distinguished.

3.1. Ion effects

When it comes to interactions of NPs with electrolytes, generally, a destabilization owing to the well-known screening of surface charges is predominantly discussed in the literature [46]. However, when totally ligand-free gold and silver, NPs were first laser-synthesized in the presence of electrolytes, stabilization occurred in the presence of NaCl [102,103]. More extensive studies with different electrolytes at varying salinities revealed that these effects are anion-specific, occurring only with chaotropic anions (Cl^-, Br^-, I^-, SCN^-), whereas kosmotropic anions (F^-, SO_4^{2-}) did not induce a stabilizing effect. For NO_3^-, the findings in the literature are inconsistent. While generally a destabilizing effect is reported for gold [95,103], at lower ionic strengths [101] and for silver [102], however, stabilization was found. It is believed that this ion adsorption significantly alters the NP's nanoenvironment, as the ions transfer their charges to the NP surface and hence increase electrostatic stabilization (figure 3*a*). These findings seem to indicate that Hofmeister effects, thoroughly described in the preceding paragraph, may also appear on curved gold interfaces. A Hofmeister series of anions for this system could be deferred, by successfully correlating the stability of gold colloids to the polarizability of the anions present during synthesis [101] (figure 3*b*). Interestingly, these effects already occur in highly diluted electrolytes in a micromolar to millimolar concentration range [31,101,102]. Specific accumulation of chaotropic anions in the nanoenvironment of NPs does not only affect colloidal stability, it also interferes with the growth mechanism of ligand-free NPs. As a result, these ions induce a size quenching effect during NP growth which was reported for gold [31,97,103] and silver NPs [102,104–106]. This means that in a micromolar concentration regime increasing ionic strengths significantly reduce NP size and their NP size distribution. It was recently proposed that size reduction in highly diluted electrolytes is directly related to the NP surface area, which can be electrostatically stabilized by the available anions [31]. A summary of the different anions and their stabilizing and size quenching effects on ligand-free gold and silver NPs is summarized in table 1. Table 1 clearly shows the suitability of anions for size quenching of ligand-free nanoparticles. Consecutively, comments are provided when ambiguous effects were reported for different ions. For example, for HCl, different stabilizing effects were found dependent on the used ionic strength (concentration) and for gold and silver nanoparticles (material). Additionally, table 1 provides literature for a more detailed study, sorted by the metals (Au, Ag) studied.

3.2. pH effects

The influence of pH on the nanoenvironment of ligand-free colloidal metal (M) NPs is mostly due to oxidation of surface atoms and a pH-dependent equilibrium between $M-O^-$/$M-OH$ and $M-OH/MOH_2^+$ species, respectively. This has

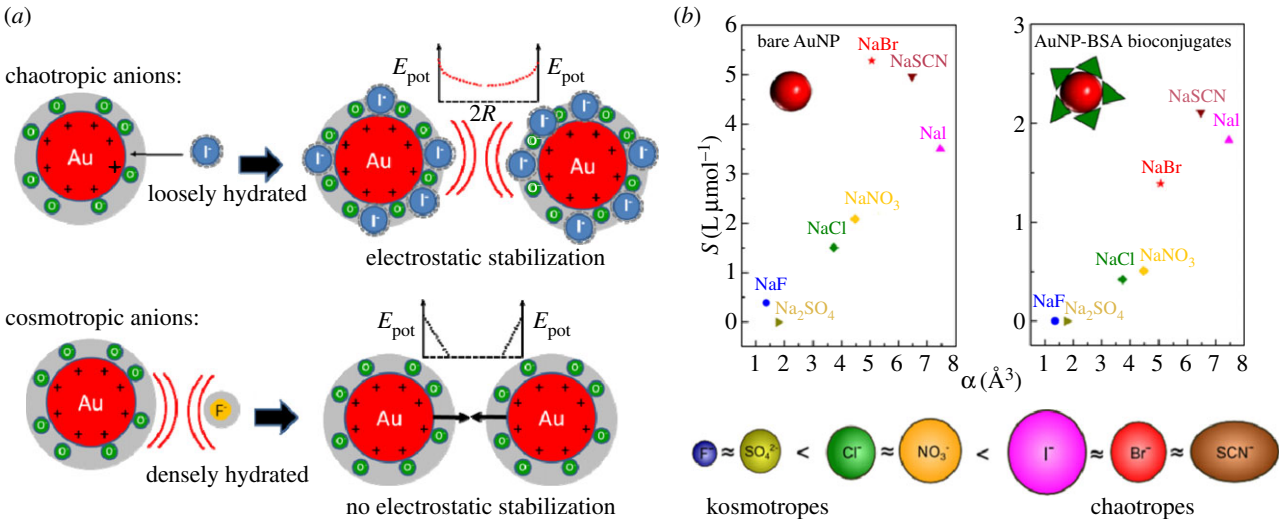

Figure 3. (*a*) Ion-specific interactions of chaotropic and kosmotropic anions in the nanoenvironment of gold NPs. The graph shows the dependence of the repulsive potential energy E_{pot} in dependence of the surface-to-surface distance $2R$ between adjacent NPs. (*b*) Colloidal stability as indicated by the slope S of the polydispersity index from UV–Vis spectroscopy, in dependence of the polarizability α of the anion, for bare Au NPs without ligand and Au NPs coated with bovine serum albumin (BSA). The resulting Hofmeister series for gold NPs is shown. Adapted from Merk *et al.* [101], to which we also refer for more details.

Table 1. Specific effects of different ions on the stability and size quenching of ligand-free Au and Ag NPs. (Signs in brackets indicate limitations or ambivalent effects found by different researchers including comments regarding possible reasons.)

ion	stabilization	size quenching	reference
F^-	—	—	Au [101]
Cl^-	(+)/(−)	(+)/(−)	Au [31,83,95,101,103]
	concentration	concentration	Ag [102,104–106]
Br^-	++	+	Au [31,101]
I^-	(++) NP etching	+	Au [95,101]
SCN^-	++	+	Au [101]
NO_3^-	(−)/(+)	(−)/(+)	Au [95,101,103]
	concentration	concentration	Ag [102]
SO_4^{2-}	—	—	Au [31,101]
PO_4^{3-}	+	+	Au [31]
NaH_2PO_4/ Na_2HPO_4	+	+	Au [31]
OH^-	+	(+)/(−)	Au [103]
		concentration	
HCl	(−)/(+)	(−)/(+)	Au [103]
	concentration, material	concentration, material	Ag [102]
$S_2O_3^{2-}$	—	—	Ag [102]

been quantitatively described in the case of SiO_2 and Al_2O_3 surfaces by the site-binding model used for solid-state based ion-sensitive sensors [107–111]. At low pH, the surface can be charged positively by the adsorption of protons (MOH_2^+), whereas it will be negatively charged at high pH owing to depletion of protons ($M–O^-$). The equilibrium of the reaction $M–O^- + 2\,H^+ \leftrightarrow M–OH + H^+ \leftrightarrow MOH_2^+$ is described by the law of mass action by the respective pK_a ($=-\log(K_a)$) values $K_{a1} = c(M–O^-) \times c(H^+)/c(M–OH)$ and $K_{a2} = c(M–OH) \times c(H^+)/c(MOH_2^+)$. Both equilibria depend on pH ($=-\log(c(H^+))$). In this way, the surface charge and hence the electrostatic stability reaches a minimum close to the isoelectric point (pI) at pH = pI [112]. This effect was frequently observed for metal oxide NPs such as ZnO [113,114], TiO_2 [115] and Al_2O_3 [116], where larger NPs owing to agglomeration were predominantly formed close to the pI value of the respective NP species. It is important to note that with metal oxides, e.g. for Al_2O_3, different hydroxide species may form. Dependent on the pH, the NPs were equilibrated, and hence different pI values may be found [117] The pI values of exemplary NP species are shown in table 2. As the presence of surface hydroxide is obvious in metal oxides, they are also found in the case of gold NPs obtained from physical synthesis routes such as laser ablation in liquid. X-ray photoelectron spectroscopy measurements confirmed that these NPs possess partially oxidized surfaces (3.3–6.6% of Au^+ and Au^{3+}) [101,120]. Fourier transform infrared spectroscopy

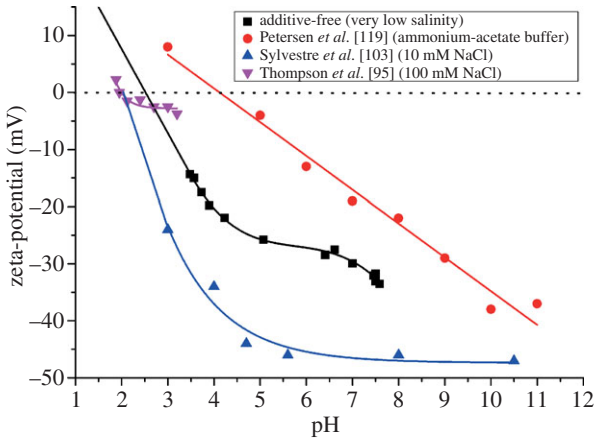

Figure 4. Ion effects on the isoelectric points of gold NPs. Zeta-potential ζ of ligand-free NPs at different pH values for the determination of the isoelectric point, as adapted from [95,103,119] as well as unpublished data (2013).

Table 2. Charge equilibrium in the nanoenvironment (pH at the isoelectric points (pI)) of exemplary ligand-free colloidal NPs.

NP species	isoelectric point (p*I*)	reference
TiO_2	6	[115]
ZnO	9	[113]
Al_2O_3	8.6 (acidic equilibration)	[117]
	5.3 (alkaline equilibration)	
AuPt	(7) indirect method	[118]
Au	2–2.5 (4.5)	[95,103,119]

measurements verified the presence of Au–O bonds on the surface [103]. An indirect verification of a p*I* value in ligand-free noble metal systems was recently found for $Au_{50}Pt_{50}$–alloy NPs which were laser-ablated at different pHs. Here, a steep increase in NP size owing to agglomeration processes was found at pH < 7 [118]. A titration of ligand-free gold NPs in order to determine the p*I* value was performed for NPs obtained from gas-phase synthesis [95] and laser ablation in liquid [103,119] by monitoring the zeta-potential at different pH values. In all cases, stabilization was found for more alkaline pH. The results from three different references and recently obtained experimental data are summarized in figure 4. In our experiments, totally additive-free gold NPs were titrated with HCl, fitted with a fourth-order polynomial, whereas linear extrapolation was used in order to determine the p*I* value. Note that Thompson *et al.* [95] originally measured the electrophoretic motility, which was transferred to the zeta-potential for better comparability, applying Smoluchowski's equation [77].

These data clearly show that additive-free gold NPs possess an isoelectric point at pH = 2.5. These findings slightly deviate from p*I*-values reported in the literature by Thompson *et al.* [95] (p*I* = 2) and Sylvestre *et al.* [103] (p*I* = 2.2). These differences may be due to high concentrations of chloride (100 and 10 mM) present during their experiments, whereas in the additive-free sample chloride, solutions with three orders of magnitude lower salinities (93 µM) were applied. As it was described in the preceding paragraph, chloride may specifically adsorb on gold NP surfaces, which increases the negative surface charge of the NPs.

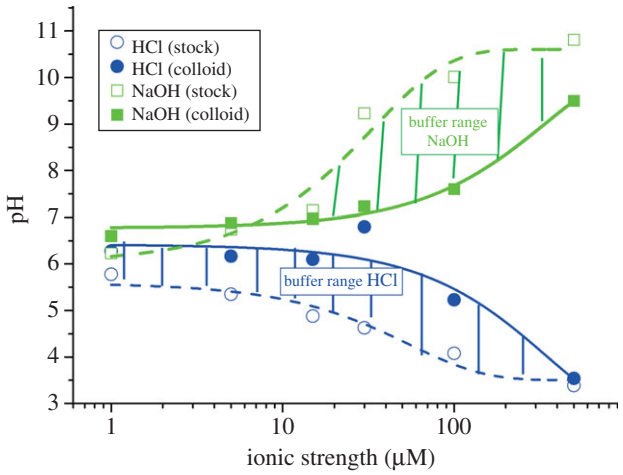

Figure 5. The buffer effect of charged NP surfaces. The pH values of ligand-free gold NP suspensions as synthesized in the presence of NaOH and HCl at varying concentrations of the respective acid (HCl) and base (NaOH; solid lines) are plotted versus the ionic strength *I* of the solution. As comparison the pH of the NaOH and HCl stock solutions was monitored as well (dashed lines).

Naturally, in these samples, more protons are necessary for charge compensation, and the isoelectric point is reached at a more acidic pH. Completely different results were obtained by Petersen *et al.* [119] where a p*I* of 4.5 was found. These deviations may be due to the fact that a system of CH_3COOH/NH_3 was used for pH adjustment. On the one hand, this approach eliminates ion effects but on the other hand, another organic ligand is added and a CH_3COO^-/CH_3COOH buffer system is formed, influencing the solution's pH. This high diversity of findings clearly illustrates that to further examine the influence of varying pH on the nanoenvironment of ligand-free gold NPs, additional ion effects need to be minimized and hence the ionic strength has to be reduced. To this end, we recently prepared NPs by pulsed laser ablation in liquid in the presence of NaOH and HCl at concentrations from 1 to 500 µM. In both cases, a significant growth quenching causing size reduction of the NPs was found compared with products synthesized in water. In case of HCl, this is most likely due to the stabilizing effect of Cl^-, blocking the gold seed's crystal growth preventing further growth. In the observed concentration regime, this effect seems to compensate the destabilization by protons reported for higher HCl concentrations [103]. For NaOH, the deprotonation of surface Au–OH groups, and the increased abundance of surface charges is the most probable cause for reduced NP size and stabilization, which is in accordance with data from literature [103]. The most interesting effect, however, was observed when the pH of the stock solution (just diluted HCl or NaCl), and the NP-containing solution was monitored during this experiment (figure 5). It was found that the pH of both NP-containing solutions synthesized in the presence of HCl and NaOH remained stable at around 6.5 up to a concentration of 30 µM, leading to a significant deviation from pH values found in the stock solution. For higher concentrations, the pH significantly deviated from the value of 6.5, though the measured values were still considerably different from the stock solutions. These findings seem to indicate that ligand-free gold NPs work as a buffer in highly diluted electrolytes, totally stabilizing the pH at 6.5 up to a proton surplus, as well as a proton deficiency of 30 µM. Apparently, the nanoenvironment of the

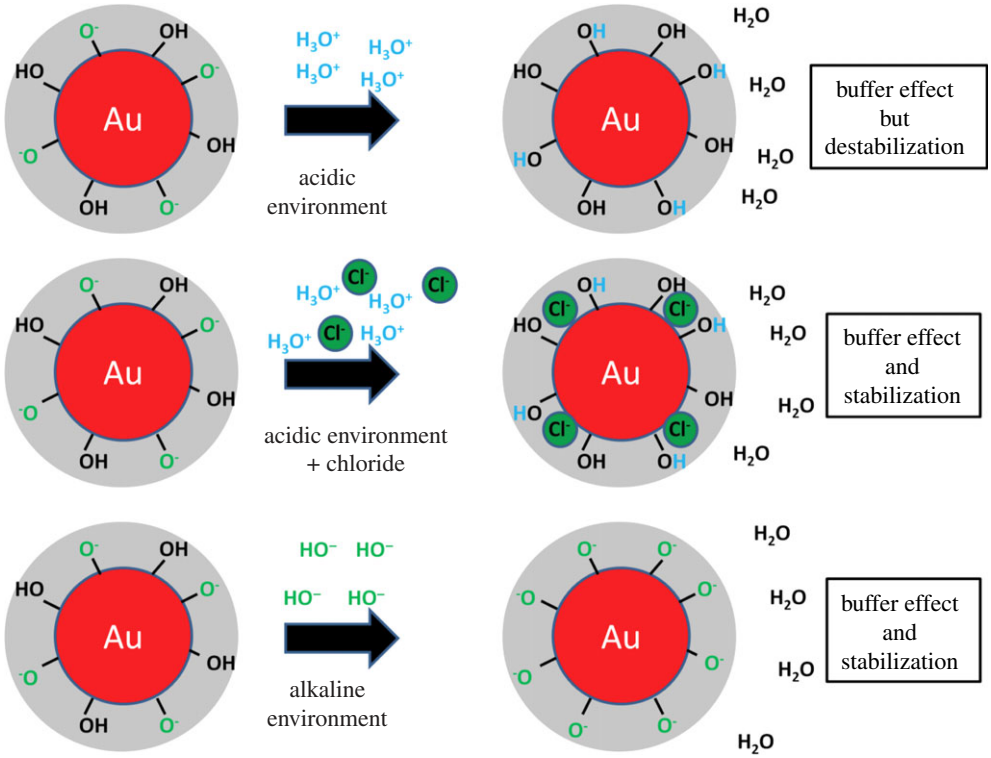

Figure 6. Buffer effect caused by the nanoenvironment of gold NPs in acidic and alkaline bulk environments.

gold NPs accumulates protons from acidic solutions and emits protons to an alkaline environment probably by changing the Au–O^-/Au–OH ratio, significantly affecting the pH of the bulk solution. This fundamental effect, that the NPs themselves and their nanoenvironment work as a buffer system, significantly affecting the bulk solution, is often neglected when working with NPs. The underlying concept is illustrated in figure 6. As a result, in 1 ml of the examined gold NP solution with an average NP core radius r_c of 4 nm and a mass concentration of 100 µg ml^{-1}, there are roughly 2.2×10^{17} gold surface atoms present, which can accumulate and emit about 30 nmol of H^+, which is equal to 1.8×10^{16} H^+ ions. Consequently, about 8% of the surface atoms take part in this buffering reaction, which is in good accordance with the literature stating that up to 6.6% of the gold surface is oxidized [101,120] and hence may carry an Au–OH or AuO^- group. In conclusion, a buffer capacity of 0.77 nmol $(H^+)/cm^2$(gold NP surface) is reached, which is very low compared with conventional buffers, though this comparison only considers pure continuum states of the environment. By contrast, the observed buffer effect is directly caused by the Gouy–Chapman layer in the nanoscopic vicinity of the NPs. Hence, such effects might be relevant in highly pH-sensitive reactions at low concentrations.

4. Effects of ion-induced nanoenvironments on the stability and the nanoenvironment of ligand-coated nanoparticles

While the concepts as described above for ligand-free metal NPs, in general, are true also for ligand-coated NPs, the situation becomes more complex. This is due to the hybrid nature of ligand-coated NPs, which besides the inorganic core also comprise an organic (ligand-)coating [21]. Now, ions in solution will be in equilibrium with several entities, not only with the originally bare NP surface of the inorganic core but also with the ligand shell, which itself can comprise different parts. In the important case of carboxylic acids as ligands, there will be the pH-dependent equilibrium $-COO^- + H^+ \leftrightarrow -COOH$ with $K_a = c(-COO^-) \times c(H^+)/c(-COOH)$. In the case of complex carboxylic acids several pK_a values can exist, which can be determined by titration experiments [121]. In case the pH is smaller than the pK_a value, the NP surface is losing its charge and predominantly comprises $-COOH$ groups, as $pK_a - pH = -\log(c(-COO^-)/c(-COOH))$. Thus, the NPs lose their colloidal stability and start to agglomerate. At alkaline solution $pH \gg pK_a$, the NP's surface on the other hand is saturated with negative charge $c(-COO^-)$ and the NPs are colloidal stable. The situation can change with other ligands, for example with positively charged ones [122]. In the case of amino terminated ligands $-NH_2 + H^+ \leftrightarrow -NH_3^+$, the NPs are charged at low, acidic pH ($-NH_3^+$, $pH \ll pK_a$), as $pK_a - pH = -\log(c(-NH_2)/c(-NH_3^+))$. In the case of high $pH \gg pK_a$, the NPs are uncharged ($-NH_2$) and thus will lose their colloidal stability. Consequently, as described before for ligand-free NPs also in the case of ligand-coated NPs, the local pH can (though not automatically) determine the surface charge of the NPs, whereby the dependence is given by the nature of the ligand. In contrast to ligand-free NPs, ligand-coated NPs can be also made with ligands comprising a permanent charge (e.g. ammonium salts, which are fully dissociated and thus permanently charged), which then have a pH-independent surface charge [53]. Most important, these NPs can be stabilized also with macromolecular ligands, such as PEG, which provides colloidal stability via steric repulsion. In this way, ligands on the NP surface introduce higher flexibility in achieving (pH-independent) colloidal stability, in particular via permanently charged ligands and/or ligands providing steric repulsion. As for ligand-free NPs, besides the charge directly associated with the NP surface (now here in particular to the ligand shell), also ligand-coated NPs comprise a diffusive cloud of charge

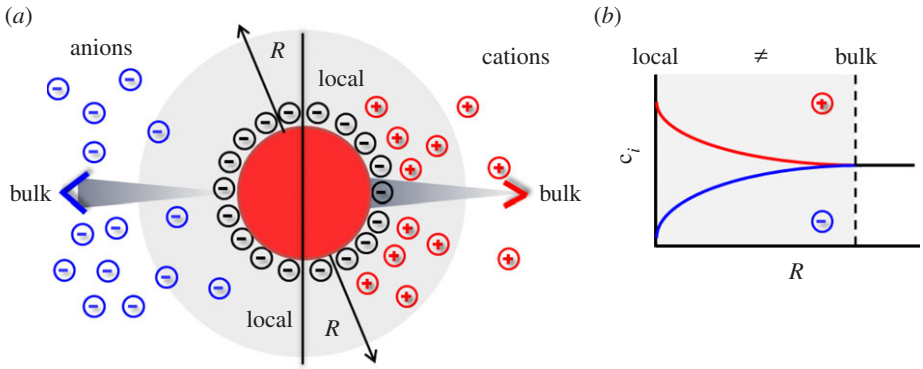

Figure 7. The concentration of ions at the surface of an NP is different from the respective bulk concentration. (*a*) In the case of negatively charged NPs (e.g. NPs with $-COO^-$ ligands) owing to Debye–Hückel screening there will be a local depletion and accumulation of anions and cations, respectively, close to the NP's surface. (*b*) The graph demonstrates schematically that the concentration c_i of ions of different species depends on the distance R from the NP surface, and is different from bulk close to NP surfaces.

by attracted counter ions according to the Gouy–Chapman model. Thus, in a similar way, the use of charged NPs produces changes in the concentration of charged species in a solution. For negatively charged NP surfaces (e.g. COO^- stabilized NPs), there is a local depletion of negatively charged analytes (i.e. anions such as OH^- or Cl^-), and a local accumulation of positively charged analytes (i.e. cations such as Na^+ or H^+; figure 7*a*, [55]). Please note that these effects are absolutely non-specific and only depend on charge and valency of the ions. There will be a screening effect by oppositely charged ions, but in case several different ions are present all of them contribute. In the case in which Na^+ ions are present, less H^+ is attracted to the surface of negatively charged NPs [55]. The opposite scenario will occur in the case in which positively charged NPs are involved [55,56]. Coming back to our main statement, this means that the local ion concentration close to the NP surface will be different from the bulk concentration (figure 7*b*), i.e. NPs influence their environment. This fact has severe effects on sensing with NPs, which will be discussed later. In the same way, this screening effect owing to the adsorption of counter-ions, together with the pH-dependent surface charge of the ligand shell, determines the colloidal stability of the NPs, i.e. the nanoenvironment affects the physico-chemical properties of the NP surface.

Unfortunately, a detailed theoretical description of the ion distribution around ligand-coated NPs is not as straight forward as for ligand-free NPs. This is due to their hybrid nature. Already, the question where the NP surface begins cannot be clearly answered [21]. The ligand shell, in general, is not homogeneous. A practical system for example can comprise hydrophobic surfactant molecules, surrounded by an amphiphilic polymer, with an additional shell of PEG [57]. This ligand shell is not completely rigid, i.e. one cannot exactly determine where the transition from one layer to the next layer (e.g. the polymer PEG interface) is located. Even the final hydrodynamic radii r_h underlie much larger distributions than the original core radius r_c. Thus, models describing the different parts of the ligand shell would need to consider distributions of respective different layers. Fortunately, distributions are not as smeared out as one may expect, as for example indicated by fluorescence resonance energy transfer measurements which revealed a relatively narrow distribution of fluorophores attached to the polymer shell around fluorescent NPs [123]. Different layers of the ligand shell can also interact in different manners with ions. Long PEG chains, for example, chelate ions such as Na^+ or K^+, and thus change the surface charge of the NPs [124]. All these effects make theoretical predictions about the quantitative ion distribution around ligand-coated NPs complicated. The starting point of such theoretical descriptions very often uses the Poisson–Boltzmann equation. It can be solved within numerical or analytical approximations as was shown for a charged hard sphere within an electrolyte solution in various studies [125–130]. More accurate models assume a permeable soft shell, e.g. consisting of a polyelectrolyte layer, around the hard sphere to approximate a potential ligand shell, although the detailed conformation of that shell is not considered [131–133]. More recent approaches are based on Monte Carlo simulations and the classical density functional theory (DFT). These allow for the consideration of the intrinsic ion volume and moreover for the treatment of the solvent molecules as the third fraction of individual components instead of a dielectric continuum [134,135]. The DFT moreover offers the possibility to consider volume displacement effects by potential ligands such as PEG attached to the NP surface [136–138].

From an experimental approach, ion-sensitive fluorophores attached to NPs are a feasible strategy to probe ion concentrations close to NP surfaces. Such fluorophores change their emission, usually the intensity of emission, dependent on the concentration of the respective ion. However, most convenient are ion-sensitive fluorophores with ratiometric detection schemes, in which not absolute intensities need to be detected, but the intensities of the emissions at two different wavelengths are compared [56,139]. This can be achieved either by fluorophores with two emission peaks [140] or by combining an ion-sensitive fluorophore which emits at one wavelength with a reference fluorophore which emits at another wavelength [56,141,142]. Thus, in order to determine the ion concentration profile around NPs, ion-sensitive fluorophores (and the reference fluorophores) need to be immobilized at different distances R to the NP surface. This can be conveniently done by using molecular spacers such as DNA [143–145] or PEG [55–57]. In order to obtain spacers providing controlled distances R, the trick lies in saturating the NP surface. In this way, the spacers are stretched (instead of forming statistical coils) and thus have defined conformation [146]. The confirmation of only a few spacer molecules per NP is in general not known. In the case of flexible spacers, they might

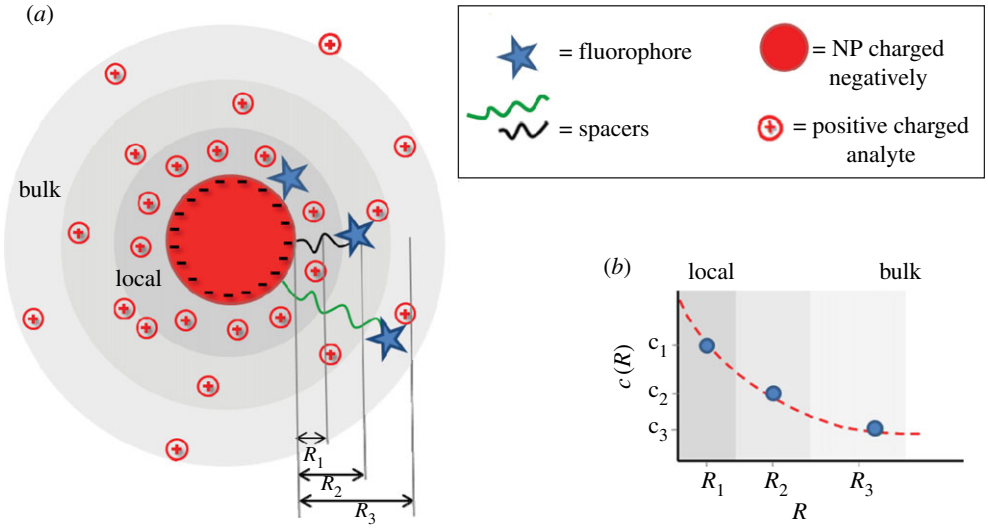

Figure 8. Scheme for measuring the distribution of ions with concentration $c(R)$ in dependence of the distance R to the NP surface.

be partly wrapped around the NP surface, or they might be dangling in solution [146]. However, in the case the NP surface is saturated with attached spacer molecules, they all will adopt similar geometry and thus lead to defined distances R. Fluorophores can be linked to the end of the spacer molecules [147,148], and by using spacers with different molecular weight the average distance between fluorophores and the NP surface can be tuned [143,149,150]. This principle has been applied to sense local H^+ [55,57] and Cl^- [56] concentrations. According to figures 7 and 8 for negatively charged NPs, higher H^+ and lower Cl^- concentrations were found close to the NP surface when compared with bulk. Thus, the response curves of the ion-sensitive fluorescence readout are shifted in the case the fluorophores are attached close to the NP surface. In the case of long enough spacers, the fluorophores are sufficiently far away from the NP surface, and thus bulk readout is obtained. This implicates that for all NP-based sensing applications one must consider that the actual environment of the NPs where the measurement takes place is different from bulk, e.g. ion concentrations at the NP surface are different from bulk values. While the fact that the local environment around NPs is different from the bulk can be seen as a potential drawback or source of complication in the field of sensors based on NPs, it could also be employed for improving the sensitivity. Here, we will suggest possible ways of exploiting this effect. One advantage of getting a higher concentration of an analyte (here in particular ions) close to the NP surface is that the NP can act not only as detector but also as preconcentration system. If the concentration of an ion in the bulk solution is extremely low, it will be hard to detect it. However, the sensitivity is increased if the ions can be preconcentrated on the surface of the NP playing with the charge density of the NP. Several articles have already been reported showing this potential use. For example, tetraalkylammonium bromide coated silver NPs have been successfully applied as electrostatic affinity probes to preconcentrate peptide mixtures in biological samples [151]. In another example detection limits as low as nanomolar concentrations were achieved using positively charged poly-L-lysine-coated silver NPs [152]. Local concentration at the NP surface hereby was achieved by the strong interaction of these NPs with the anionic bilirubin molecules. In the case of working with ion-sensitive fluorophores, the strategy would be to locate the fluorophore on the NP surface (e.g. by integrating the fluorophore directly in the polymer shell) for measuring the local concentration (of oppositely charged ions), which would be much higher than the bulk concentration due to the preconcentration effect. Using appropriate calibration curves then could be used to calculate the preconcentration factor achieved with the particular configuration in order to finally determine the bulk concentration of the target ions.

5. Conclusion

The local environment of NPs has a profound interaction with the surface of NPs, which induce that the physicochemical properties of both, the environment and the surface can be mutually altered. The surface of NPs creates a special local environment, with different properties compared with the bulk. Owing to different repulsion/adsorption effects local molecular concentrations around the NP, surface can be quite different from bulk concentrations. This has strong effects on NP-based sensors, as those probe concentrations of the local environment, and not from the bulk. In the other direction, the surface charge of NPs is determined by the presence of ions in the local nanoenvironment. Via reaction with ligands or even with the bare NP surface, this regulates the surface charge of NPs and thus also their colloidal stability. These effects may be particularly pronounced when they are studied in highly pure ligand-free systems. Here, next to continuum effects, ion-specific interactions occur in the particle's nanoenvironment which may significantly alter particle properties such as stability and may even affect the composition of the bulk phase.

Acknowledgements. D.J. acknowledges a PhD fellowship for the Basque Country, Spain.

Funding statement. This work was supported by the DFG (graduate research school 1782 to W.J.P. and the project REPROTOX within priority programme SPP1313 to S.B.). C.C.C. acknowledges a postdoctoral fellowship from the Alexander von Humboldt Foundation.

References

1. Pelaz B, Charron G, Pfeiffer C, Zhao YL, de la Fuente JM, Liang XJ, Parak WJ, del Pino P. 2013 Interfacing engineered nanoparticles with biological systems: anticipating adverse nanobio interactions. *Small* **9**, 1573–1584. (doi:10.1002/smll.201201229)
2. Singh D, Kumar S, Singh SC, Lal B, Singh NB. 2012 Applications of liquid assisted pulsed laser ablation synthesized TiO2 nanoparticles on germination, growth and biochemical parameters of *Brassica oleracea* var. Capitata. *Sci. Adv. Mater.* **4**, 522–531. (doi:10.1166/sam.2012.1313)
3. Corradini E, de Moura MR, Mattoso LHC. 2010 A preliminary study of the incorparation of NPK fertilizer into chitosan nanoparticles. *Express. Polymer Lett.* **4**, 509–515. (doi:10.3144/expresspolymlett.2010.64)
4. Khodakovskaya MV, de Silva K, Biris AS, Dervishi E, Villagarcia H. 2012 Carbon nanotubes induce growth enhancement of tobacco cells. *ACS Nano* **6**, 2128–2135. (doi:10.1021/nn204643g)
5. Perelshtein I *et al*. 2013 Chitosan and chitosan–ZnO-based complex nanoparticles: formation, characterization, and antibacterial activity. *J. Mater. Chem. B* **1**, 1968–1976. (doi:10.1039/c3tb00555k)
6. Chernousova S, Epple M. 2013 Silver as antibacterial agent: ion, nanoparticle, and metal. *Angew. Chem. Int. Ed.* **52**, 1636–1653. (doi:10.1002/anie.201205923)
7. Hajipour MJ, Fromm KM, Ashkarran AA, Aberasturi DJd, Larramendi IRd, Rojo T, Serpooshan V, Parak WJ, Mahmoudi M. 2012 Antibacterial properties of nanoparticles. *Trends Biotechnol.* **30**, 499–511. (doi:10.1016/j.tibtech.2012.06.004)
8. Ojea-Jimenez I, Lopez X, Arbiol J, Puntes V. 2012 Citrate-coated gold nanoparticles as smart scavengers for mercury(II) removal from polluted waters. *ACS Nano* **6**, 2253–2260. (doi:10.1021/nn204313a)
9. Venkatanarasimhan S, Raghavachari D. 2013 Epoxidized natural rubber–magnetite nanocomposites for oil spill recovery. *J. Mater. Chem. A* **1**, 868–876. (doi:10.1039/c2ta00445c)
10. Zhu Q, Tao F, Pan Q. 2010 Fast and selective removal of oils from water surface via highly hydrophobic core-shell Fe_2O_3@C nanoparticles under magnetic field. *ACS Appl. Mater. Interfaces* **2**, 3141–3146. (doi:10.1021/am1006194)
11. Arvizo RR, Bhattacharyya S, Kudgus RA, Giri K, Bhattacharya R, Mukherjee P. 2012 Intrinsic therapeutic applications of noble metal nanoparticles: past, present and future. *Chem. Soc. Rev.* **41**, 2943–2970. (doi:10.1039/c2cs15355f)
12. Parveen S, Misra R, Sahoo SK. 2012 Nanoparticles: a boon to drug delivery, therapeutics, diagnostics and imaging. *Nanomedicine* **8**, 147–166. (doi:10.1016/j.nano.2011.05.016)
13. Garcia-Bennett A, Nees M, Fadeel B. 2011 In search of the holy grail: folate-targeted nanoparticles for cancer therapy. *Biochem. Pharmacol.* **81**, 976–984. (doi:10.1016/j.bcp.2011.01.023)
14. Al-Jamal WT, Kostarelos K. 2011 Liposomes: from a clinically established drug delivery system to a nanoparticle platform for theranostic nanomedicine. *Acc. Chem. Res.* **44**, 1094–1104. (doi:10.1021/ar200105p)
15. Peteiro-Cartelle J, Rodríguez-Pedreira M, Zhang F, Gil PR, Mercato LLd, Parak WJ. 2009 One example on how colloidal nano- and microparticles could contribute to medicine. *Nanomedicine* **4**, 967–979. (doi:10.2217/nnm.09.84)
16. Batley GE, Kirby JK, McLaughlin MJ. 2013 Fate and risks of nanomaterials in aquatic and terrestrial environments. *Acc. Chem. Res.* **46**, 854–862. (doi:10.1021/ar2003368)
17. Peters R *et al*. 2012 Presence of nano-sized silica during *in vitro* digestion of foods containing silica as a food additive. *ACS Nano* **6**, 2441–2451. (doi:10.1021/nn204728k)
18. Zhang P, Ma YH, Zhang ZY, He X, Zhang J, Guo Z, Tai RZ, Zhao YL, Chai ZF. 2012 Biotransformation of ceria nanoparticles in cucumber plants. *ACS Nano* **6**, 9943–9950. (doi:10.1021/nn303543n)
19. Hernandez-Viezcas JA *et al*. 2013 *In situ* synchrotron X-ray fluorescence mapping and speciation of CeO_2 and ZnO nanoparticles in soil cultivated soybean (glycine max). *ACS Nano* **7**, 1415–1423. (doi:10.1021/nn305196q)
20. Hoecke KV, Schamphelaer KACD, Ali Z, Zhang F, Elsaesser A, Rivera_Gil P, Parak WJ, Smagghe G, Janssen CR. 2013 *In vitro* ecotoxicity and uptake of polymer coated gold nanoparticles. *Nanotoxicology* **7**, 37–47. (doi:10.3109/17435390.2011.626566)
21. Rivera Gil P *et al*. 2013 The challenge to relate the physicochemical properties of colloidal nanoparticles to their cytotoxicity. *Acc. Chem. Res.* **46**, 743–749. (doi:10.1021/ar300039j)
22. Fu FN, Fuller MP, Singh BR. 1993 Use of Fourier-transform infrared attenuated total reflectance spectroscopy for the study of surface-adsorption of proteins. *Appl. Spectrosc.* **47**, 98–102. (doi:10.1366/0003702934048451)
23. Peng ZG, Hidajat K, Uddin MS. 2004 Adsorption of bovine serum albumin on nanosized magnetic particles. *J. Colloid Interface Sci.* **271**, 277–283. (doi:10.1016/j.jcis.2003.12.022)
24. Verma A, Uzun O, Hu YH, Hu Y, Han HS, Watson N, Chen SL, Irvine DJ, Stellacci F. 2008 Surface-structure-regulated cell-membrane penetration by monolayer-protected nanoparticles. *Nat. Mater.* **7**, 588–595. (doi:10.1038/nmat2202)
25. Hung A, Mwenifumbo S, Mager M, Kuna JJ, Stellacci F, Yarovsky I, Stevens MM. 2011 Ordering surfaces on the nanoscale: implications for protein adsorption. *J. Am. Chem. Soc.* **133**, 1438–1450. (doi:10.1021/ja108285u)
26. Cedervall T, Lynch I, Lindman S, Berggård T, Thulin E, Nilsson H, Dawson KA, Linse S. 2007 Understanding the nanoparticle-protein corona using methods to quantify exchange rates and affinities of proteins for nanoparticles. *Proc. Natl Acad. Sci. USA* **104**, 2050–2055. (doi:10.1073/pnas.0608582104)
27. Linse S, Cabaleiro-Lago C, Xue W-F, Lynch I, Lindman S, Thulin E, Radford SE, Dawson KA. 2007 Nucleation of protein fibrillation by nanoparticles. *Proc. Natl Acad. Sci. USA* **104**, 8691–8696. (doi:10.1073/pnas.0701250104)
28. Lynch I, Dawson KA. 2008 Protein–nanoparticle interactions. *Nano Today* **3**, 40–47. (doi:10.1016/S1748-0132(08)70014-8)
29. Röcker C, Pötzl M, Zhang F, Parak WJ, Nienhaus GU. 2009 A quantitative fluorescence study of protein monolayer formation on colloidal nanoparticles. *Nat. Nanotechnol.* **4**, 577–580. (doi:10.1038/nnano.2009.195)
30. Jiang X, Weise S, Hafner M, Röcker C, Zhang F, Parak WJ, Nienhaus GU. 2010 Quantitative analysis of the protein corona on FePt nanoparticles formed by transferrin binding. *J. R. Soc. Interface* **7**, S5–S13. (doi:10.1098/rsif.2009.0272.focus)
31. Rehbock C, Merk V, Gamrad L, Streubel R, Barcikowski S. 2013 Size control of laser-fabricated surfactant-free gold nanoparticles with highly diluted electrolytes and their subsequent bioconjugation. *Phys. Chem. Chem. Phys.* **15**, 3057–3067. (doi:10.1039/c2cp42641b)
32. Gebauer JS, Malissek M, Simon S, Knauer SK, Maskos M, Stauber RH, Peukert W, Treuel L. 2012 Impact of the nanoparticle–protein corona on colloidal stability and protein structure. *Langmuir* **28**, 9673–9679. (doi:10.1021/la301104a)
33. Kittler S *et al*. 2010 The influence of proteins on the dispersability and cell-biological activity of silver nanoparticles. *J. Mater. Chem.* **20**, 512–518. (doi:10.1039/b914875b)
34. Shemetov AA, Nabiev I, Sukhanova A. 2012 Molecular interaction of proteins and peptides with nanoparticles. *ACS Nano* **6**, 4585–4602. (doi:10.1021/nn300415x)
35. Deng ZJ, Liang M, Toth I, Monteiro MJ, Minchin RF. 2012 Molecular interaction of poly(acrylic acid) gold nanoparticles with human fibrinogen. *ACS Nano* **6**, 8962–8969. (doi:10.1021/nn3029953)
36. Goy-Lopez S, Juarez J, Alatorre-Meda M, Casals E, Puntes VF, Taboada P, Mosquera V. 2012 Physicochemical characteristics of protein–NP bioconjugates: the role of particle curvature and solution conditions on human serum albumin conformation and fibrillogenesis inhibition. *Langmuir* **28**, 9113–9126. (doi:10.1021/la300402w)
37. Amin F, Yushchenko DA, Montenegro JM, Parak WJ. 2012 Integration of organic fluorophores in the surface of polymer-coated colloidal nanoparticles for sensing the local polarity of the environment. *ChemPhysChem* **13**, 1030–1035. (doi:10.1002/cphc.201100901)
38. Fatin-Rouge N, Starchev K, Buffle J. 2004 Size effects on diffusion processes within agarose gels. *Biophys. J.* **86**, 2710–2719. (doi:10.1016/S0006-3495(04)74325-8)

39. Sperling RA, Liedl T, Duhr S, Kudera S, Zanella M, Lin C-AJ, Chang WH, Braun D, Parak WJ. 2007 Size determination of (bio-) conjugated water-soluble colloidal nanoparticles: a comparison of different techniques. *J. Phys. Chem. C* **111**, 11 552–11 559. (doi:10.1021/jp070999d)
40. Bell NC, Minelli C, Tompkins J, Stevens MM, Shard AG. 2012 Emerging techniques for submicrometer particle sizing applied to Stöber silica. *Langmuir* **28**, 10 860–10 872. (doi:10.1021/la301351k)
41. Lees EE, Gunzburg MJ, Nguyen T-L, Howlett GJ, Rothacker J, Nice EC, Clayton AHA, Mulvaney P. 2008 Experimental determination of quantum dot size distributions, ligand packing densities, and bioconjugation using analytical ultracentrifugation. *Nano Lett.* **8**, 2883–2890. (doi:10.1021/nl801629f)
42. Monopoli MP, Walczyk D, Campbell A, Elia G, Lynch I, Bombelli FB, Dawson KA. 2011 Physical–chemical aspects of protein corona: relevance to *in vitro* and *in vivo* biological impacts of nanoparticles. *J. Am. Chem. Soc.* **133**, 2525–2534. (doi:10.1021/ja107583h)
43. Maffre P, Nienhaus K, Amin F, Parak WJ, Nienhaus GU. 2011 Characterization of protein adsorption onto FePt nanoparticles using dual-focus fluorescence correlation spectroscopy. *Beilstein J. Nanotechnol.* **2**, 374–383. (doi:10.3762/bjnano.2.43)
44. Mahmoudi M *et al*. 2013 Temperature: the 'ignored' factor at the nanobio interface. *ACS Nano* **7**, 6555–6562. (doi:10.1021/nn305337c)
45. He Q, Zhang J, Shi J, Zhu Z, Zhang L, Bu W, Guo L, chen Y. 2010 The effect of PEGylation of mesoporous silica nanoparticles on nonspecific binding of serum proteins and cellular responses. *Biomaterials* **31**, 1085–1092. (doi:10.1016/j.biomaterials.2009.10.046)
46. Pellegrino T, Kudera S, Liedl T, Javier AM, Manna L, Parak WJ. 2005 On the development of colloidal nanoparticles towards multifunctional structures and their possible use for biological applications. *Small* **1**, 48–63. (doi:10.1002/smll.200400071)
47. Zhang X, Servos MR, Liu J. 2012 Ultrahigh nanoparticle stability against salt, pH, and solvent with retained surface accessibility via depletion stabilization. *J. Am. Chem. Soc.* **134**, 9910–9913. (doi:10.1021/ja303787e)
48. Ravikumar C, Kumar S, Bandyopadhyaya R. 2012 Aggregation of dextran coated magnetic nanoparticles in aqueous medium: experiments and Monte Carlo simulation. *Colloids Surf. A, Physicochem. Eng. Aspects* **403**, 1–6. (doi:10.1016/j.colsurfa.2012.02.007)
49. Debye P, Hückel E. 1923 Zur Theorie der Elektrolyte. *Phys. Z* **24**, 185–206.
50. Huynh KA, Chen KL. 2011 Aggregation kinetics of citrate and polyvinylpyrrolidone coated silver nanoparticles in monovalent and divalent electrolyte solutions. *Environ. Sci. Technol.* **45**, 5564–5571. (doi:10.1021/es200157h)
51. Li X, Lenhart JJ, Walker HW. 2012 Aggregation kinetics and dissolution of coated silver nanoparticles. *Langmuir* **28**, 1095–1104. (doi:10.1021/la202328n)
52. Gebauer JS, Treuel L. 2011 Influence of individual ionic components on the agglomeration kinetics of silver nanoparticles. *J. Colloid Interface Sci.* **354**, 546–554. (doi:10.1016/j.jcis.2010.11.016)
53. Hühn D *et al*. 2013 Polymer-coated nanoparticles interacting with proteins and cells: focusing on the sign of the net charge. *ACS Nano* **7**, 3253–3263. (doi:10.1021/nn3059295)
54. Caballero-Díaz E, Pfeiffer C, Kastl L, Rivera-Gil P, Simonet B, Valcárcel M, Jiménez-Lamana J, Laborda F, Parak WJ. 2013 The toxicity of silver nanoparticles depends on their uptake by cells and thus on their surface chemistry. *Part. Part. Syst. Charact.* **30**, 1079–1085. (doi:10.1002/ppsc.201300215)
55. Zhang F, Ali Z, Amin F, Feltz A, Oheim M, Parak WJ. 2010 Ion and pH sensing with colloidal nanoparticles: influence of surface charge on sensing and colloidal properties. *ChemPhysChem* **11**, 730–735. (doi:10.1002/cphc.200900849)
56. Riedinger A, Zhang F, Dommershausen F, Röcker C, Brandholt S, Nienhaus GU, Koert U, Parak WJ. 2010 Ratiometric optical sensing of chloride ions with organic fluorophore–gold nanoparticle hybrids: a systematic study of distance dependency and the influence of surface charge. *Small* **6**, 2590–2597. (doi:10.1002/smll.201000868)
57. Zhang F, Lees E, Amin F, Rivera Gil P, Yang F, Mulvaney P, Parak WJ. 2011 Polymer-coated nanoparticles: a universal tool for biolabelling experiments. *Small* **7**, 3113–3127. (doi:10.1002/smll.201100608)
58. Derjaguin B, Sidorenkov G. 1941 Thermoosmosis at ordinary temperatures and its analogy with the thermomechanical effect in helium II. *C. R. Acad. Sci.* **32**, 622–626.
59. Verwey EJW, Overbeek JTG. 1948 *Theory of the stability of lyophobic colloids*. Amsterdam, The Netherlands: Elsevier.
60. Ninham BW. 1999 On progress in forces since the DLVO theory. *Adv. Colloid Interface Sci.* **83**, 1–17. (doi:10.1016/S0001-8686(99)00008-1)
61. Bauduin P, Nohmie F, Touraud D, Neueder R, Kunz W, Ninham BW. 2006 Hofmeister specific-ion effects on enzyme activity and buffer pH: horseradish peroxidase in citrate buffer. *J. Mol. Liq.* **123**, 14–19. (doi:10.1016/j.molliq.2005.03.003)
62. Hofmeister F. 1888 Zur Lehre von der Wirkung der Salze - Zweite Mittheilung. *Arch. Exp. Pathol. Pharm* **24**, 247–260. (doi:10.1007/BF01918191)
63. Medda L, Barse B, Cugia F, Bostrom M, Parsons DF, Ninham BW, Monduzzi M, Salis A. 2012 Hofmeister challenges: ion binding and charge of the BSA protein as explicit examples. *Langmuir* **28**, 16 355–16 363. (doi:10.1021/la3035984)
64. Vrbka L, Jungwirth P, Bauduin P, Touraud D, Kunz W. 2006 Specific ion effects at protein surfaces: a molecular dynamics study of bovine pancreatic trypsin inhibitor and horseradish peroxidase in selected salt solutions. *J. Phys. Chem. B* **110**, 7036–7043. (doi:10.1021/jp0567624)
65. Gao P, Weaver MJ. 1986 Metal adsorbate vibrational frequencies as a probe of surface bonding—halides and pseudohalides at gold electrodes. *J. Phys. Chem.* **90**, 4057–4063. (doi:10.1021/j100408a045)
66. Magnussen OM, Ocko BM, Wang JX, Adzic RR. 1996 *In situ* X-ray diffraction and STM studies of bromide adsorption on Au(111) electrodes. *J. Phys. Chem.* **100**, 5500–5508. (doi:10.1021/jp953281j)
67. Magnussen OM, Ocko BM, Adzic RR, Wang JX. 1995 X-ray-diffraction studies of ordered chloride and bromide monolayers at the Au(111)-solution interface. *Phys. Rev. B* **51**, 5510–5513. (doi:10.1103/PhysRevB.51.5510)
68. Biggs S, Mulvaney P, Zukoski CF, Grieser F. 1994 Study of anion adsorption at the gold–aqueous solution interface by atomic-force microscopy. *J. Am. Chem. Soc.* **116**, 9150–9157. (doi:10.1021/ja00099a033)
69. Verwey EJW, De Boer JH. 1936 Surface oxide films. *Recueil Des Travaux Chimiques Des Pays-Bas* **55**, 675–687. (doi:10.1002/recl.19360550806)
70. Stern O. 1924 Zur Theorie der Elektrolytischen Doppelschicht. *Z. Elektr.* **30**, 508–516.
71. Rhee IH, Dzombak DA. 1998 Surface complexation Gouy–Chapman modeling of binary and ternary cation exchange. *Langmuir* **14**, 935–943. (doi:10.1021/la9700331)
72. Helmholtz H. 1879 Studien über elektrische Grenzschichten. *Wiedemanns Anal. Phys. Chem.* **7**, 337–382.
73. Chapman DL. 1913 A contribution to the theory of electrocapillarity. *Philos. Mag.* **25**, 475–481.
74. Gouy M. 1909 Sur la constitution de la charge electrique a la surface d'un electrolyte. *C.R. Acad. Sci.* **149**, 654–657.
75. Gouy M. 1910 Sur la constitution de la charge electrique a la surface d'un electrolyte. *J. Phys.* **9**, 457–468.
76. Doane TL, Chuang CH, Hill RJ, Burda C. 2012 Nanoparticle zeta-potentials. *Acc. Chem. Res.* **45**, 317–326. (doi:10.1021/ar200113c)
77. Smoluchowski M. 1906 Zur kinetischen Theorie der Brownschen Molekularbewegung und der Suspensionen. *Ann. Phys.* **21**, 756–780. (doi:10.1002/andp.19063261405)
78. Hückel E. 1924 Die Kataphorese der Kugel. *Phys. Z* **25**, 204–210.
79. Henry DC. 1931 The cataphoresis of suspended particles. I. The equation of cataphoresis. *Proc. R. Soc. Lond. A* **133**, 106–129. (doi:10.1098/rspa.1931.0133)
80. Doane TL, Burda C. 2012 The unique role of nanoparticles in nanomedicine: imaging, drug delivery and therapy. *Chem. Soc. Rev.* **41**, 2885–2911. (doi:10.1039/c2cs15260f)
81. Baersch N, Jakobi J, Weiler S, Barcikowski S. 2009 Pure colloidal metal and ceramic nanoparticles from high-power picosecond laser ablation in water and acetone. *Nanotechnology* **20**, 445603. (doi:10.1088/0957-4484/20/44/445603)
82. Barcikowski S, Compagnini G. 2013 Advanced nanoparticle generation and excitation by lasers in

liquids. *Phys. Chem. Chem. Phys.* **15**, 3022–3026. (doi:10.1039/c2cp90132c)

83. Amendola V, Meneghetti M. 2013 What controls the composition and the structure of nanomaterials generated by laser ablation in liquid solution? *Phys. Chem. Chem. Phys.* **15**, 3027–3046. (doi:10.1039/c2cp42895d)
84. Zeng HB, Du XW, Singh SC, Kulinich SA, Yang SK, He JP, Cai WP. 2012 Nanomaterials via laser ablation/irradiation in liquid: a review. *Adv. Funct. Mater.* **22**, 1333–1353. (doi:10.1002/adfm.201102295)
85. Keller F, Feist M, Nirschl H, Dorfler W. 2010 Investigation of the nonlinear effects during the sedimentation process of a charged colloidal particle by direct numerical simulation. *J. Colloid Interface Sci.* **344**, 228–236. (doi:10.1016/j.jcis.2009.12.032)
86. Lo Nostro P, Ninham BW. 2012 Hofmeister phenomena: an update on ion specificity in biology. *Chem. Rev.* **112**, 2286–2322. (doi:10.1021/cr200271j)
87. Tavares FW, Bratko D, Blanch HW, Prausnitz JM. 2004 Ion-specific effects in the colloid–colloid or protein–protein potential of mean force: role of salt–macroion van der Waals interactions. *J. Phys. Chem. B* **108**, 9228–9235. (doi:10.1021/jp037809t)
88. dos Santos AP, Levin Y. 2012 Ions at the water–oil interface: interfacial tension of electrolyte solutions. *Langmuir* **28**, 1304–1308. (doi:10.1021/la204036e)
89. Collins KD. 1997 Charge density-dependent strength of hydration and biological structure. *Biophys. J.* **72**, 65–76. (doi:10.1016/S0006-3495(97)78647-8)
90. Collins KD. 2004 Ions from the Hofmeister series and osmolytes: effects on proteins in solution and in the crystallization process. *Methods* **34**, 300–311. (doi:10.1016/j.ymeth.2004.03.021)
91. Manciu M, Ruckenstein E. 2003 Specific ion effects via ion hydration: I. Surface tension. *Adv. Colloid Interface Sci.* **105**, 63–101. (doi:10.1016/S0001-8686(03)00018-6)
92. Kolb DM, Franke C. 1989 Surface-states at the metal electrolyte interface. *Appl. Phys. A, Mater. Sci. Process.* **49**, 379–387. (doi:10.1007/BF00615020)
93. Gutsch A, Muhlenweg H, Kramer M. 2005 Tailor-made nanoparticles via gas-phase synthesis. *Small* **1**, 30–46. (doi:10.1002/smll.200400021)
94. Kruis FE, Fissan H, Peled A. 1998 Synthesis of nanoparticles in the gas phase for electronic, optical and magnetic applications—a review. *J. Aerosol Sci.* **29**, 511–535. (doi:10.1016/S0021-8502 (97)10032-5)
95. Thompson DW, Collins IR. 1992 Electrical-properties of the gold aqueous–solution interface. *J. Colloid Interface Sci.* **152**, 197–204. (doi:10.1016/0021-9797(92)90019-I)
96. Menendez-Manjon A, Barcikowski S. 2011 Hydrodynamic size distribution of gold nanoparticles controlled by repetition rate during pulsed laser ablation in water. *Appl. Surf. Sci.* **257**, 4285–4290. (doi:10.1016/j.apsusc.2010.12.037)
97. Amendola V, Meneghetti M. 2009 Laser ablation synthesis in solution and size manipulation of noble metal nanoparticles. *Phys. Chem. Chem. Phys.* **11**, 3805–3821. (doi:10.1039/b900654k)
98. Semaltianos NG. 2010 Nanoparticles by laser ablation. *Crit. Rev. Solid State Mater. Sci.* **35**, 105–124. (doi:10.1080/10408431003788233)
99. Tilaki RM, Zad AI, Mahdavi SM. 2007 The effect of liquid environment on size and aggregation of gold nanoparticles prepared by pulsed laser ablation. *J. Nanoparticle Res.* **9**, 853–860. (doi:10.1007/s11051-006-9143-0)
100. Kabashin AV, Meunier M. 2003 Synthesis of colloidal nanoparticles during femtosecond laser ablation of gold in water. *J. Appl. Phys.* **94**, 7941–7943. (doi:10.1063/1.1626793)
101. Merk CVR, Rehbock C, Becker F, Hagemann U, Nienhaus H, Barcikowski S. 2013 *In situ* non-DLVO stabilization of surface-free, plasmonic gold nanoparticles: the effect of Hofmeister's anions. *Langmuir*. (doi:10.1021/la404556a)
102. Siskova K, Vlckova B, Turpin PY, Fayet C. 2008 Ion-specific effects on laser ablation of silver in aqueous electrolyte solutions. *J. Phys. Chem. C* **112**, 4435–4443. (doi:10.1021/jp076680a)
103. Sylvestre JP, Poulin S, Kabashin AV, Sacher E, Meunier M, Luong JHT. 2004 Surface chemistry of gold nanoparticles produced by laser ablation in aqueous media. *J. Phys. Chem. B* **108**, 16 864–16 869. (doi:10.1021/jp047134+)
104. Srnova I, Prochazka M, Vlckova B, Stepanek J, Maly P. 1998 Surface-enhanced Raman scattering-active systems prepared from Ag colloids laser-ablated in chemically-modified aqueous media. *Langmuir* **14**, 4666–4670. (doi:10.1021/la9707540)
105. Bae CH, Nam SH, Park SM. 2002 Formation of silver nanoparticles by laser ablation of a silver target in NaCl solution. *Appl. Surf. Sci.* **197**, 628–634. (doi:10.1016/S0169-4332(02)00430-0)
106. Prochazka M, Mojzes P, Stepanek J, Vlckova B, Turpin PY. 1997 Probing applications of laser ablated Ag colloids in SERS spectroscopy: improvement of ablation procedure and SERS spectral testing. *Anal. Chem.* **69**, 5103–5108. (doi:10.1021/ac970683+)
107. Bousse L, Rooij NFd, Bergveld P. 1983 The influence of counter-ion adsorption on the ψ_0/pH characteristics of insulator surfaces. *Surf. Sci.* **135**, 479–496. (doi:10.1016/0039-6028(83)90237-6)
108. Bousse L, Mostarshed S. 1991 The zeta potential of silicon nitride thin films. *J. Electroanal. Chem.* **302**, 269–274. (doi:10.1016/0022-0728(91)85046-R)
109. Raiteri R, Martinoia S, Grattarola M. 1996 pH-dependent charge density at the insulator–electrolyte interface probed by a scanning force microscope. *Biosens. Bioelectron.* **11**, 1009–1017. (doi:10.1016/0956-5663(96)87660-3)
110. van Hal REG, Eijkel JCT, Bergveld P. 1995 A novel description of ISFET sensitivity with the buffer capacity and double-layer capacitance as key parameters. *Sensors Actuators B, Chem.* **24–25**, 201–205. (doi:10.1016/0925-4005(95)85043-0)
111. Healy TW, Chan D, White LR. 1980 Colloidal behaviour of materials with ionizable group surfaces. *Pure Appl. Chem.* **52**, 1207–1219. (doi:10.1351/pac198052051207)
112. Parks GA. 1965 The isoelectric points of solid oxides, solid hydroxides, and aqueous hydroxo complex systems. *Chem. Rev.* **65**, 177–198. (doi:10.1021/cr60234a002)
113. Liufu S, Xiao H, Li Y. 2004 Investigation of PEG adsorption on the surface of zinc oxide nanoparticles. *Powder Technol.* **145**, 20–24. (doi:10.1016/j.powtec.2004.05.007)
114. He C, Sasaki T, Usui H, Shimizu Y, Koshizaki N. 2007 Fabrication of ZnO nanoparticles by pulsed laser ablation in aqueous media and pH-dependent particle size: an approach to study the mechanism of enhanced green photoluminescence. *J. Photochem. Photobiol. A Chem.* **191**, 66–73. (doi:10.1016/j.jphotochem.2007.04.006)
115. Sugiyama M, Okazaki H, Koda S. 2002 Size and shape transformation of TiO_2 nanoparticles by irradiation of 308-nm laser beam. *Jpn J. Appl. Phys. Part 1 Regular Pap. Short Not. Rev. Pap.* **41**, 4666–4674. (doi:10.1143/JJAP.41.4666)
116. Al-Mamun SA, Nakajima R, Ishigaki T. 2013 Tuning the size of aluminum oxide nanoparticles synthesized by laser ablation in water using physical and chemical approaches. *J. Colloid Interface Sci.* **392**, 172–182. (doi:10.1016/j.jcis.2012.10.027)
117. Gulicovski JJ, Cerovic LS, Milonjin SK. 2008 Point of zero charge and isoelectric point of alumina. *Mater. Manuf. Process.* **23**, 615–619. (doi:10.1080/10426910802160668)
118. Zhang JM, Oko DN, Garbarino S, Imbeault R, Chaker M, Tavares AC, Guay D, Ma DL. 2012 Preparation of PtAu alloy colloids by laser ablation in solution and their characterization. *J. Phys. Chem. C* **116**, 13 413–13 420. (doi:10.1021/jp302485g)
119. Petersen S, Barchanski A, Taylor U, Klein S, Rath D, Barcikowski S. 2011 Penetratin-conjugated gold nanoparticles—design of cell-penetrating nanomarkers by femtosecond laser ablation. *J. Phys. Chem. C* **115**, 5152–5159. (doi:10.1021/jp1093614)
120. Muto H, Yamada K, Miyajima K, Mafune F. 2007 Estimation of surface oxide on surfactant-free gold nanoparticles laser-ablated in water. *J. Phys. Chem. C* **111**, 17 221–17 226. (doi:10.1021/jp075582m)
121. Charron G, Hühn D, Perrier A, Cordier L, Pickett CJ, Nann T, Parak WJ. 2012 On the use of pH titration to quantitatively characterize colloidal nanoparticles. *Langmuir* **28**, 15 141–15 149. (doi:10.1021/la302570s)
122. Geidel C, Schmachtel S, Riedinger A, Pfeiffer C, Müllen K, Klapper M, Parak WJ. 2011 A general synthetic approach for obtaining cationic and anionic inorganic nanoparticles via encapsulation in amphiphilic copolymers. *Small* **7**, 2929–2934. (doi:10.1002/smll.201100509)
123. Yakovlev AV *et al*. 2009 Wrapping nanocrystals with an amphiphilic polymer preloaded with fixed amounts of fluorophore generates FRET-based nanoprobes with a controlled donor/acceptor ratio. *Langmuir* **25**, 3232–3239. (doi:10.1021/la8038347)

124. Sperling RA, Pellegrino T, Li JK, Chang WH, Parak WJ. 2006 Electrophoretic separation of nanoparticles with a discrete number of functional groups. *Adv. Funct. Mater.* **16**, 943–948. (doi:10.1002/adfm.200500589)
125. Hoskin NE. 1953 Solution to the Poisson–Boltzmann equation for the potential distribution in the double layer of a single spherical colloidal particle. *Trans. Faraday Soc.* **49**, 1471–1477. (doi:10.1039/tf9534901471)
126. Brenner SL, Roberts RE. 1973 Variational solution of Poisson–Boltzmann equation for a spherical colloidal particle. *J. Phys. Chem.* **77**, 2367–2370. (doi:10.1021/j100639a001)
127. White LR. 1977 Approximate analytic solution of the Poisson–Boltzmann equation for a spherical colloidal particle. *J. Chem. Soc. Faraday Trans. II* **73**, 577–596. (doi:10.1039/f29777300577)
128. Ohshima H, Healy TW, White LR. 1982 Accurate analytic expressions for the surface-charge density surface-potential relationship and double-layer potential distribution for a spherical colloidal particle. *J. Colloid Interface Sci.* **90**, 17–26. (doi:10.1016/0021-9797(82)90393-9)
129. Ohshima H. 2004 Potential distribution around a charged spherical colloidal particle in a medium containing its counterions and a small amount of added salts. *Colloid Polym. Sci.* **282**, 1185–1191. (doi:10.1007/s00396-004-1072-9)
130. Zhou S, Zhang G. 2012 Approximate analytic solution of the nonlinear Poisson–Boltzmann equation for spherical colloidal particles immersed in a general electrolyte solution. *Colloid Polym. Sci.* **290**, 1511–1526. (doi:10.1007/s00396-012-2683-1)
131. Lopez-Garcia JJ, Horno J, Grosse C. 2001 Numerical solution of the Poisson–Boltzmann equation for suspended charged particles surrounded by a charged permeable membrane. *Phys. Chem. Chem. Phys.* **3**, 3754–3760. (doi:10.1039/b101701m)
132. Ohshima H. 2003 Potential distribution around a polyelectrolyte-coated spherical particle in a salt-free medium. *J. Colloid Interface Sci.* **268**, 429–434. (doi:10.1016/j.jcis.2003.08.020)
133. Ohshima H. 2008 Donnan potential and surface potential of a spherical soft particle in an electrolyte solution. *J. Colloid Interface Sci.* **323**, 92–97. (doi:10.1016/j.jcis.2008.03.021)
134. Patra CN. 2009 Molecular solvent model of spherical electric double layers: a systematic study by Monte Carlo simulations and density functional theory. *J. Phys. Chem. B* **113**, 13 980–13 987. (doi:10.1021/jp907790t)
135. Patra CN. 2010 Structure of spherical electric double layers containing mixed electrolytes: a systematic study by Monte Carlo simulations and density functional theory. *J. Phys. Chem. B* **114**, 10 550–10 557. (doi:10.1021/jp1042975)
136. Wu JZ, Li ZD. 2007 Density-functional theory for complex fluids. *Annu. Rev. Phys. Chem.* **58**, 85–112. (doi:10.1146/annurev.physchem.58.032806.104650)
137. Yu YX, Wu JZ, Gao GH. 2004 Density-functional theory of spherical electric double layers and zeta potentials of colloidal particles in restricted-primitive-model electrolyte solutions. *J. Chem. Phys.* **120**, 7223–7233. (doi:10.1063/1.1676121)
138. Rex S, Zuckermann MJ, Lafleur M, Silvius JR. 1998 Experimental and Monte Carlo simulation studies of the thermodynamics of polyethyleneglycol chains grafted to lipid bilayers. *Biophys. J.* **75**, 2900–2914. (doi:10.1016/S0006-3495(98)77732-X)
139. Arduini M, Mancin F, Tecilla P, Tonellato U. 2007 Self-organized fluorescent nanosensors for ratiometric Pb^{2+} detection. *Langmuir* **23**, 8632–8636. (doi:10.1021/la700971n)
140. Page LE, Zhang X, Jawaid AM, Snee PT. 2011 Detection of toxic mercury ions using a ratiometric CdSe/ZnS nanocrystal sensor. *Chem. Commun.* **47**, 7773–7775. (doi:10.1039/c1cc11442e)
141. Doussineau T, Smaihi M, Mohr GJ. 2009 Two-dye core/shell zeolite nanoparticles: a new tool for ratiometric pH measurements. *Adv. Funct. Mater.* **19**, 117–122. (doi:10.1002/adfm.200800718)
142. Ali Z *et al*. 2011 Multifunctional nanoparticles for dual imaging. *Anal. Chem.* **83**, 2877–2882. (doi:10.1021/ac103261y)
143. Obliosca JM, Wang P-C, Tseng F-G. 2012 Probing quenched dye fluorescence of Cy3–DNA–Au nanoparticle hybrid conjugates using solution and array platforms. *J. Colloid Interface Sci.* **371**, 34–41. (doi:10.1016/j.jcis.2011.12.026)
144. Diaz JA, Grewer DM, Gibbs-Davis JM. 2012 Tuning ratios, densities, and supramolecular spacing in bifunctional DNA-modified gold nanoparticles. *Small* **8**, 873–883. (doi:10.1002/smll.201101922)
145. Chhabra R, Sharma J, Wang H, Zou S, Lin S, Yan H, Lindsay S, Liu Y. 2009 Distance-dependent interactions between gold nanoparticles and fluorescent molecules with DNA as tunable spacers. *Nanotechnology* **20**, 485201. (doi:10.1088/0957-4484/20/48/485201)
146. Pellegrino T, Sperling RA, Alivisatos AP, Parak WJ. 2007 Gelelectrophoresis of gold–DNA nanoconjugates. *J. Biomed. Biotechnol.* **2007,** 1–9. (doi:10.1155/2007/26796)
147. Shenoy D, Fu W, Li J, Crasto C, Jones G, DiMarzio C, Sridhar S, Amiji M. 2006 Surface functionalization of gold nanoparticles using hetero-bifunctional poly(ethylene glycol) spacer for intracellular tracking and delivery. *Int. J. Nanomed.* **1**, 51–57. (doi:10.2147/nano.2006.1.1.51)
148. Liu W, Howarth M, Greytak AB, Zheng Y, Nocera DG, Ting AY, Bawendi MG. 2008 Compact biocompatible quantum dots functionalized for cellular imaging. *J. Am. Chem. Soc.* **130**, 1274–1284. (doi:10.1021/ja076069p)
149. Dulkeith E, Ringler M, Klar TA, Feldmann J, Javier AM, Parak WJ. 2005 Gold nanoparticles quench fluorescence by phase induced radiative rate suppression. *Nanoletters* **5**, 585–589. (doi:10.1021/nl0480969)
150. Nagatoishi S, Nojima T, Galezowska E, Gluszynska A, Juskowiak B, Takenaka S. 2007 Fluorescence energy transfer probes based on the guanine quadruplex formation for the fluorometric detection of potassium ion. *Anal. Chim. Acta* **581**, 125–131. (doi:10.1016/j.aca.2006.08.010)
151. Sudhir P-R, Shrivas K, Zhou Z-C, Wu H-F. 2008 Single drop microextraction using silver nanoparticles as electrostatic probes for peptide analysis in atmospheric pressure matrix-assisted laser desorption/ionization mass spectrometry and comparison with gold electrostatic probes and silver hydrophobic probes. *Rapid Commun. Mass Spectrom.* **22**, 3076–3086. (doi:10.1002/rcm.3710)
152. Marsich L, Bonifacio A, Mandal S, Krol S, Beleites C, Sergo V. 2012 Poly-L-lysine-coated silver nanoparticles as positively charged substrates for surface-enhanced Raman scattering. *Langmuir* **28**, 13 166–13 171. (doi:10.1021/la302383r)